IEEE Access
Multidisciplinary ⋮ Rapid Review ⋮ Open Access Journal

Received 11 April 2024, accepted 26 May 2024, date of publication 29 May 2024, date of current version 5 June 2024.

Digital Object Identifier 10.1109/ACCESS.2024.3406855

RESEARCH ARTICLE

Design and Optimization of Control System for More Electric Aircraft Power Systems Using Adaptive Tabu Search Algorithm Based on State-Variables-Averaging Model

RATAPON PHOSUNG, KONGPAN AREERAK, (Member, IEEE), AND KONGPOL AREERAK, (Member, IEEE)
School of Electrical Engineering, Institute of Engineering, Suranaree University of Technology, Nakhon Ratchasima 30000, Thailand
Corresponding author: Kongpan Areerak (kongpan@sut.ac.th)

This research project is supported by National Research Council of Thailand (NRCT): (Contact No. N41A661128), in part by the Royal Golden Jubilee Ph.D. Program (RGJ), and in part by Suranaree University of Technology (SUT).

ABSTRACT An important reflection of the overall efficiency, reliability, and passenger safety of a more electric aircraft (MEA) is the output performance of its electrical power system (EPS) controller. This output performance encompasses the rise time, setting time, and percent undershoot of the voltage across the capacitor bank. Therefore, this article presents an optimal controller design using an artificial intelligence method called the adaptive tabu search (ATS) algorithm. The state-variables-averaging model is applied with the ATS algorithm to reduce computational time. Moreover, stability analysis based on the eigenvalue theorem is used as the penalty condition during the searching process to avoid unstable operation. The output performance of the proposed controller design is superior to that of the conventional controller design. All design results are verified by good agreement with MATLAB and hardware-in-the-loop (HIL) simulations.

INDEX TERMS More electric aircraft, vector control, state-variables-averaging model, adaptive tabu search algorithm.

I. INTRODUCTION

According to published concepts for more electric aircraft (MEA) [1], [2], [3], [4], [5], [6], aircraft performance optimization, flight reliability improvement, and passenger safety improvement are essential tasks. Altering the MEA controller design is an approach with strong potential to accomplish these tasks. Artificial intelligence (AI) techniques are required to achieve the optimal output performance of the MEA's electrical power system (EPS) controller in terms of the rise time, setting time, and percent undershoot of the voltage across the capacitor bank. AI can be used for controller design and many other functions. For example, AI has been applied to the design of active power filters for the adaptive tabu search (ATS) algorithm [7] and genetic algorithm [8], power flow optimization based on particle swarm optimization [9], ant colony search algorithm [10], antenna array design using artificial bee colony algorithm [11], and the application of the ATS algorithm to instability mitigation [12]. However, one of the crucial problems that arises when applying AI techniques to the EPS of MEA is the simulation time. This is because the simulation of EPS using software packages such as PSIM and MATLAB causes huge computational time due to switching behavior. Thus, a time-invariant model is necessary and sufficient for the controller design. There are several reasonable methods for deriving the time-invariant model of EPS. The generalized state-space averaging modeling technique [13], [14] has been universally used for single-phase rectifiers of AC distribution systems and the power converters of DC distribution systems. The direct quadrature (DQ) approach [1], [2], [6], [12], [15], [16] is suitable for power converters in three-phase AC

The associate editor coordinating the review of this manuscript and approving it for publication was Engang Tian.

distribution systems. The nonlinear average-value method modeling technique [17] has been applied to analyze 6- and 12-pluse diode rectifiers.

Based on a literature review, the AI technique called the ATS algorithm is selected for use in the present study because it was mathematically proven in [19] to achieve convergence and escape the local solution. As for the modeling technique, the DQ approach is applied to derive the system model because the MEA EPS system considered in the present study consists of an active front-end (AFE) rectifier in three-phase AC distribution systems. Unfortunately, most loads on the MEA are power converters with controls, which behave as constant power loads. These loads act as negative impedance that can significantly degrade system stability, resulting in undesirable output performance. Consequently, stability analysis must be included in the searching process as a penalty condition. The eigenvalue theorem [1], [2], [6], [12], [15], [16], [18] based on small-signal stability analysis is applied with the dynamic model for stability analysis in the present study. The ATS algorithm uses its stability analysis mechanism to search the MEA EPS controller parameters until it reaches the acceptable condition. Under the stable operating state, the output performance of the MEA EPS is better when using the controller designed by the ATS design method than when using the controller designed by the conventional design method. Previous research publications have not reported the application of an AI technique for designing the control system, including the voltage compensator, of modern MEA EPS [4]. Good agreement among the theoretical design results, MATLAB simulation results, and hardware-in-the-loop (HIL) simulation results verify the design approach proposed in this study.

The proposed design process based on the ATS algorithm has the following main advantages:

- The DC bus voltage response of MEA EPS obtained when using the controller designed by the ATS algorithm method is better than that obtained when using the controller designed by the conventional design method. Moreover, the application of an AI technique for designing the control system, including the voltage compensator, of updated MEA EPS has not yet been reported.
- A short computational time can be achieved using the state-variables-averaging model because the switching action of the power converter can be eliminated. It is a beneficial tool and is suitable for obtaining an optimal controller design using AI techniques, wherein system responses are iteratively and continuously calculated.
- A stability assessment mechanism based on the eigenvalue theorem is integrated into design processes to avoid the unstable margin of MEA EPS. Hence, controllers designed using the proposed method can perform better with confirmed stability.
- The HIL simulation technique is used to validate the proposed design concepts. This validation confirms that the proposed controller design can be implemented using a real TMDSDOCK28335 board.
- Other AI algorithms, e.g., artificial bee colony, ant colony optimization, and flower pollination algorithms, can be applied to achieve an optimal design using the same process described in this article.

This article is structured as follows. In Section II, a single-generator-single-bus DC distribution MEA EPS and its key control parameters are introduced. The modeling of the MEA EPS system using the DQ approach is detailed in Section III. In Section IV, the ATS algorithm, including the stability analysis mechanism during the searching process, is applied to determine the controller parameters under load variation conditions. The validation of the theoretical design results by MATLAB and HIL simulations is presented in Section V. Finally, Section VI concludes this article.

II. STUDIED MEA EPS CONFIGURATION

A simplified architecture MEA, the single-generator-single bus DC distribution MEA EPS [6], [16] illustrated in Fig. 1, is considered in this study. It consists of a permanent magnet synchronous generator (PMSG) with parasitic parameters (represented by $R_{s,abc}$ and $L_{s,abc}$), an AFE rectifier, a DC link capacitor (represented by C_{dc}), a DC transmission line (represented by R_c and L_c), a bus capacitor or capacitor bank (represented by C_b), resistive loads (represented by R_L), and an ideal CPL. The resistive loads are used to represent a wing deicing system, and the ideal CPL refers to most electrical power loads on the MEA, such as the actively regulated power converter. The rated powers of R_L ($P_{RL,rated}$) and CPL ($P_{CPL,rated}$) are determined to be 7 kW and 38 kW, respectively. Consequently, the rated power of the studied system (P_{rated}) in Fig. 1 is equal to 45 kW ($P_{RL,rated} + P_{CPL,rated}$). The control structure, depicted by the dashed line in Fig. 1 and detailed in Fig. 3, is the classical vector controller on the dq-axis, which can be separated into an inner loop and an outer loop. K_{pd}, K_{id}, K_{pq}, and K_{iq} are the cascaded proportional–integral (PI) controller parameters of the inner loop; these parameters control the inductor current on the d-axis (I_d) and the inductor current on the q-axis (I_q). K_{pv} and K_{iv} are the PI controller parameters of the outer loop; these parameters regulate the voltage across the DC link capacitor (V_{dc}) and the voltage across the capacitor bank (V_b), ensuring that both are in the range 250–280 V (determined using the MIL-STD-704F standard [20] after defining the nominal voltage, V_b^*, as 270 V). K_d is the droop controller parameter (individual droop gain) of the outer loop and is responsible for sharing the power and current from the PMSG to all loads on the MEA. K_t is the voltage compensator parameter [1] (global droop gain) of the outer loop, and it is responsible for preventing or reducing voltage drop due to the droop controller's operating behavior. To determine the optimal controller parameters, the ATS algorithm is used to tune K_{pd}, K_{id}, K_{pq}, K_{iq}, K_{pv}, K_{iv}, K_d, and K_t via the state-variables-averaging model until the optimal output performance is obtained. Unfortunately, an ideal CPL acts as a negative impedance that can directly reduce system stability. Reduced system stability may result in huge oscillations of voltage

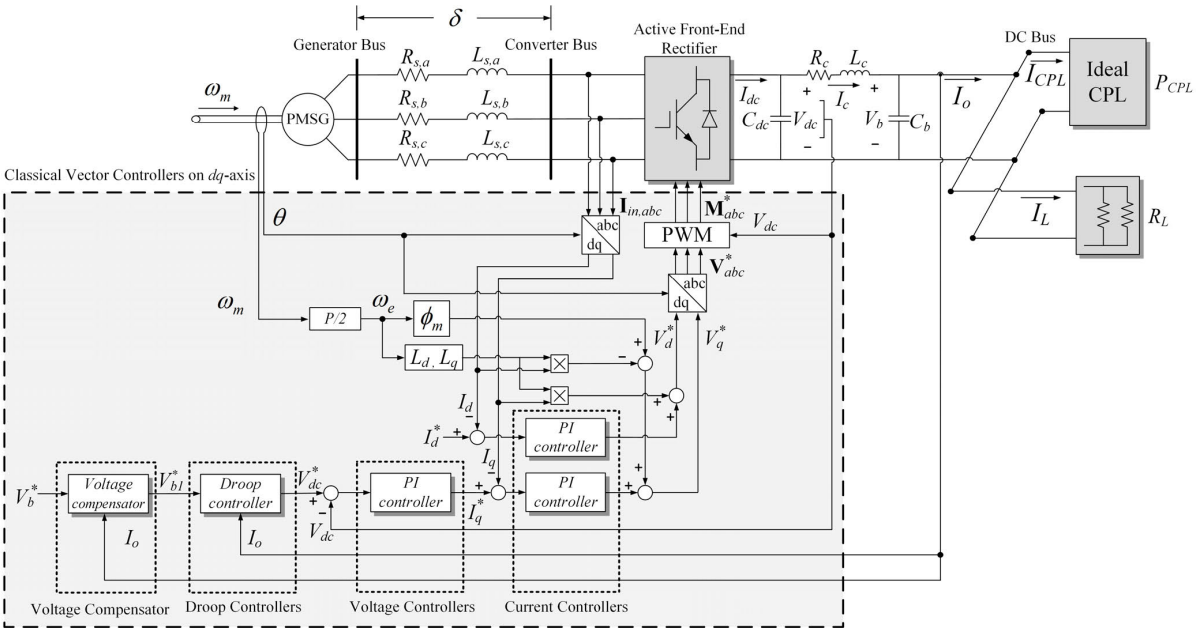

FIGURE 1. Representative DC distribution of MEA EPS.

TABLE 1. The parameters of MEA EPS.

Parameter	Value	Description
R_s	1.058 mΩ	Stator resistance
L_s	99 µH	Stator inductance
L_d	99 µH	Inductance on d-axis
L_q	99 µH	Inductance on q-axis
ϕ_m	0.03644 V·s/rad	Flux linkage
p	6	Poles
ω_e	$2\pi \times 400$ rad/s	Electrical rotor angular velocity
C_{dc}	1 mF	DC link capacitor
cable length	10 m	Length of DC transmission line
R_c	6 mΩ	DC transmission line resistance
L_c	2 µH	DC transmission line inductance
C_b	0.5 mF	Capacitor bank
R_L	10 Ω	resistive load
I_d^*	0 A	Reference stator current on d-axis
V_b^*	270 V	Nominal voltage

and current responses, potentially causing these responses to become out of control. Hence, the stability assessment mechanism should be integrated into the searching process. Additional details on how to design the MEA EPS controller using the AI approach and stability assessment are provided in Section IV. The system parameters are given in Table 1.

III. MODELING OF REPRESENTATIVE MEA EPS

As mentioned in Section II, an MEA EPS controller can be designed using the state-variables-averaging model and the ATS algorithm, hereafter referred to as the ATS design method. Thus, the establishment of a time-invariant model that is easy to use and suitable for designing system controllers is essential. Referring to the literature review in Section I, the DQ modeling method is selected to derive

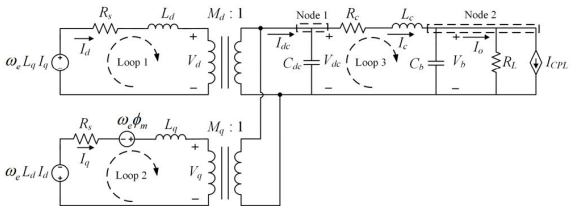

FIGURE 2. Equivalent circuit on the dq-axis of MEA EPS under open-loop operation.

the state-variables-averaging model of MEA EPS without the control system, where the PMSG and the IGBT module are mathematically analyzed as dynamic equations and transformers, respectively, on the dq frame. The resulting equivalent circuit of the MEA without closed-loop control is presented in Fig. 2. After applying Kirchhoff's voltage law and Kirchhoff's current law to Fig. 2, the dynamic model in the form of differential equations is obtained and presented in (1). More details on how to derive the mathematical model using the DQ modeling technique can be found in [16].

$$\begin{cases} \dot{I}_d = -\dfrac{R_s}{L_d} I_d + \omega_e I_q - \dfrac{M_d}{L_d} V_{dc} \\ \dot{I}_q = -\omega_e I_d - \dfrac{R_s}{L_q} I_q - \dfrac{M_q}{L_q} V_{dc} + \dfrac{\omega_e \phi_m}{L_q} \\ \dot{V}_{dc} = \dfrac{3M_d}{2C_{dc}} I_d + \dfrac{3M_q}{2C_{dc}} I_q - \dfrac{1}{C_{dc}} I_c \\ \dot{I}_c = \dfrac{1}{L_c} V_{dc} - \dfrac{R_c}{L_c} I_c - \dfrac{1}{L_c} V_b \\ \dot{V}_b = \dfrac{1}{C_b} I_c - \dfrac{1}{R_L C_b} V_b - \dfrac{P_{CPL}}{C_b V_b} \end{cases} \tag{1}$$

where M_d and M_q are the time-invariant switching functions of the IGBT module on a dq-axis. The model in (1) is time-invariant.

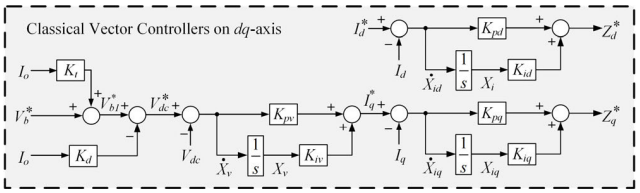

FIGURE 3. Vector controllers on dq-axis for closed-loop operation of MEA EPS.

Next, the MEA EPS model under closed-loop operation is considered. Figure 3 shows a block diagram of classical vector control on the dq-axis, in which X_{id} of the I_d control loop, X_{iq} of the I_q control loop, and X_v of the V_{dc} control loop are defined as new state variables of the model. According to the control structure shown in Fig. 3, the control signals (Z_d^* and Z_q^*) and reference modulation index on the dq-axis (M_d^* and M_q^*) are calculated using (2) and (3), respectively. Under the closed-loop operation of the MEA EPS, M_d and M_q in (1) become M_d^* and M_q^* in (3). After substituting M_d^* and M_q^* for M_d and M_q and adding all new state variables of controllers, the nonlinear model of the system shown in Fig. 1 derived from the DQ approach is expressed in (4), as shown at the bottom of the next page.

The mathematical model given in (4) is a beneficial tool for computing the desired system responses of the controller designed by the ATS design method because of its accuracy and short computational time [21], [22]. For stability analysis during the design process, the eigenvalue theorem based on the linear time-invariant (LTI) model is a suitable tool. Therefore, the first-order term of the Taylor series expansion is used to transform the nonlinear model in (4) into the LTI model in (5).

$$\begin{cases} Z_d^* = -K_{pd}I_d + K_{id}X_{id} + K_{pd}I_d^* \\ Z_q^* = -K_{pq}I_q - K_{pv}K_{pq}V_{dc} + K_{iv}K_{pq}X_v \\ \quad +K_{iq}X_{iq} + K_{pv}K_{pq}V_b^* \\ \qquad + \dfrac{K_{pv}K_{pq}(K_t - K_d)V_b}{R_L} + \dfrac{K_{pv}K_{pq}P_{CPL}(K_t - K_d)}{R_L} \end{cases} \tag{2}$$

$$\begin{cases} M_d^* = \left(\dfrac{1}{V_{dc}}\right)\left(Z_d^* + \omega_e L_q I_q\right) \\ M_q^* = \left(\dfrac{1}{V_{dc}}\right)\left(Z_q^* - \omega_e L_d I_d + \omega_e \phi_m\right) \end{cases} \tag{3}$$

$$\begin{cases} \dot{\delta\mathbf{x}} = \mathbf{A}(\mathbf{x_0}, \mathbf{u_0})\delta\mathbf{x} + \mathbf{B}(\mathbf{x_0}, \mathbf{u_0})\delta\mathbf{u} \\ \delta\mathbf{y} = \mathbf{C}(\mathbf{x_0}, \mathbf{u_0})\delta\mathbf{x} + \mathbf{D}(\mathbf{x_0}, \mathbf{u_0})\delta\mathbf{u} \end{cases} \tag{5}$$

where matrixes A, B, C, and D are the Jacobean matrixes of the MEA EPS depending on the system operation point. The details of $\delta\mathbf{x}$, $\delta\mathbf{u}$, $\delta\mathbf{y}$, A, B, C, and D can be found in Appendix.

To validate the mathematical models, an exact topological simulation was conducted using MATLAB/SimPowerSystem

TABLE 2. J value results of conventional design and ATS design method.

Vector controller parameters/J value	Design method	
	Conventional method	ATS method
K_{pd}	−1.9895	−1.1167
K_{id}	−1563.3453	−17846.259
K_{pq}	−1.9895	−0.84887
K_{iq}	−1563.3453	−15350.0928
K_{pv}	3.5744	5.3025
K_{iv}	2807.3541	4772.5019
K_d	0.06	0.0571
K_t	0.06	0.0571
J	1.0	0.6861

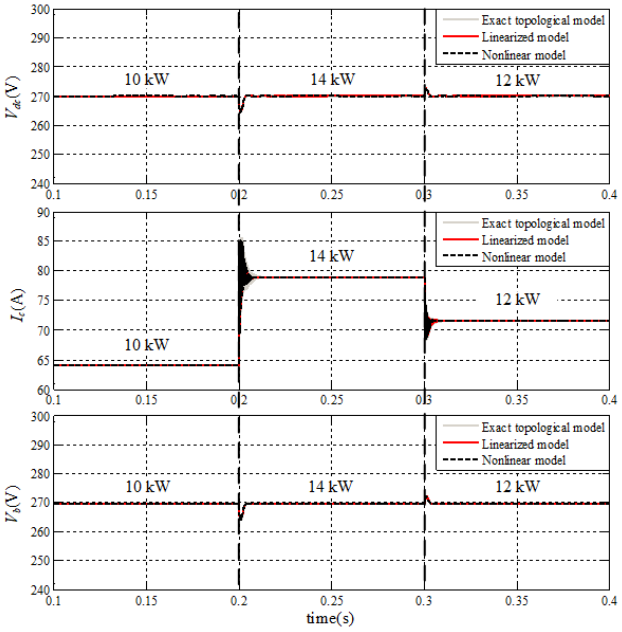

FIGURE 4. Validation of nonlinear and LTI dynamic models.

with the system parameters in Table 1 and the controller parameters in Table 2. The controller parameters for model validation are designed by using the conventional design method, which will be explained in Section IV. The model validation results when the CPL is changed from 10 kW to 14 kW and 12 kW are shown in Fig. 4. These results confirm that the nonlinear and LTI models provide good accuracy.

To determine the benefit of the state-variables-averaging model, the computational time of the simulation is plotted in Fig. 4. Simulation by the exact topological model consumes 18.84 s, whereas simulations by the nonlinear and linearized models consume 0.63 s and 0.25 s, respectively. Therefore, the computational time savings are 96.67% and 98.66% when the system is simulated using the proposed nonlinear and linearized averaging models, respectively. The short simulation time is useful for the ATS design method because the ATS algorithm must perform iterative simulations during the controller design process.

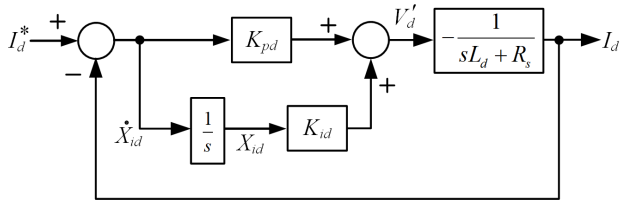

FIGURE 5. Block diagram of current loop control.

IV. OPTIMAL MEA EPS CONTROLLER DESIGN

The controllers designed for the MEA EPS using the conventional design method and the proposed ATS design method are detailed in this section.

A. CONVENTIONAL DESIGN METHOD

The conventional design method for vector controllers on the dq-axis uses the characteristic polynomial of the standard second-order system to design the PI controllers for both current and voltage loop controls.

1) CURRENT LOOP CONTROL

Figure 5 shows the block diagram of the current loop control of the studied MEA EPS, which is used to design the controllers for regulating the inductor current on the d-axis (I_d) and the q-axis (I_q). Only the design procedure of the current loop control on the d-axis will be described in this section because the loop controls on the d-axis and q-axis are identical. The closed-loop transfer function of the block diagram in Fig. 5 is expressed by (6).

$$\frac{I_d}{I_d^*} = -\frac{K_{pd}s + K_{id}}{L_d s^2 + \left(R_s - K_{pd}\right)s - K_{id}} \tag{6}$$

After comparing the denominators of (6) and the standard second-order system in (7), the equations for the parameters K_{pd} and K_{id} are established and presented in (8).

$$T = \frac{\omega_n^2}{s^2 + 2\zeta\omega_n s + \omega_n^2} \tag{7}$$

$$\begin{cases} K_{pd} = R_s - 2\zeta_i\omega_{ni}L_d \\ K_{id} = -L_d\omega_{ni}^2 \end{cases} \tag{8}$$

The equations used for designing the current loop control on the d-axis can also be used for designing the current loop control on the q-axis. The equations for calculating K_{pq} and K_{iq} are presented in (9).

$$\begin{cases} K_{pd} = R_s - 2\zeta_i\omega_{ni}L_d \\ K_{id} = -L_d\omega_{ni}^2 \end{cases} \tag{9}$$

where $\omega_{ni} = 2\pi \times f_{ni}$.

2) VOLTAGE LOOP CONTROL

Figure 6 shows the block diagram of the voltage (V_{dc}) loop control of the MEA EPS, which is used to design the controller to regulate the voltage across the DC link capacitor (V_{dc}). The closed-loop transfer function of the block diagram, presented in Fig. 6, is expressed by (10).

$$\frac{V_{dc}}{V_{dc}^*} = \frac{3m\left(K_{pv}s + K_{iv}\right)}{4C_{dc}s^2 + 3mK_{pv}s + 3mK_{iv}} \tag{10}$$

Using the same procedure implemented for designing the current loop control, the equations for designing the PI controller of the voltage loop, K_{pv} and K_{iv}, are established and expressed in (11).

$$\begin{cases} K_{pv} = \dfrac{8\zeta_v\omega_{nv}C_{dc}}{3m} \\ K_{iv} = \dfrac{4C_{dc}\omega_{nv}^2}{3m} \end{cases} \tag{11}$$

where $\omega_{nv} = 2\pi \times f_{nv}$.

$$\begin{cases} \dot{I}_d = \dfrac{(K_{pd} - R_s)}{L_d}I_d - \dfrac{K_{id}}{L_d}X_{id} - \dfrac{K_{pd}}{L_d}I_d^* \\ \dot{I}_q = \dfrac{(K_{pd} - R_s)}{L_q}I_q + \dfrac{K_{pv}K_{pq}}{L_q}V_{dc} - \dfrac{K_{pv}K_{pq}(K_t - K_d)}{L_qR_L}V_b - \dfrac{K_{iq}}{L_q}X_{iq} - \dfrac{K_{pv}K_{pq}P_{CPL}(K_t - K_d)}{L_q} \cdot \dfrac{1}{V_b} - \dfrac{K_{iv}K_{pq}}{L_q}X_v \\ \quad - \dfrac{K_{pv}K_{pq}}{L_q}V_b^* \\ \dot{V}_{dc} = \dfrac{3}{2C_{dc}} \cdot \dfrac{1}{V_{dc}} \cdot \Big[-K_{pd}I_d^2 + K_{id}I_dX_{id} + K_{pd}I_dI_d^* - K_{pq}I_q^2 + \omega_e\phi_mI_q - K_{pv}K_{pq}I_qV_{dc} + \dfrac{K_{pv}K_{pq}(K_t - K_d)}{R_L}I_qV_b \\ \quad + \dfrac{K_{pv}K_{pq}P_{CPL}(K_t - K_d)}{L_q} \cdot \dfrac{I_q}{V_b} + K_{iv}K_{pq}I_qX_v + K_{iq}I_qX_{iq} + K_{pv}K_{pq}I_qV_b^*\Big] - \dfrac{1}{C_{dc}}I_c \\ \dot{I}_c = \dfrac{1}{L_c}V_{dc} - \dfrac{R_c}{L_c}I_c - \dfrac{1}{L_c}V_b \\ \dot{V}_b = \dfrac{1}{C_b}I_c - \dfrac{1}{R_LC_b}V_b - \dfrac{P_{CPL}}{C_b} \cdot \dfrac{1}{V_b} \\ \dot{X}_v = -V_{dc} + \dfrac{(K_t - K_d)}{R_L}V_b + (K_t - K_d)P_{CPL} \cdot \dfrac{1}{V_b} + V_b^* \\ \dot{X}_{id} = -I_d + I_d^* \\ \dot{X}_{iq} = -I_q - K_{pv}V_{dc} + \dfrac{K_{pv}(K_t - K_d)}{R_L}V_b + K_{pv}(K_t - K_d)P_{CPL} \cdot \dfrac{1}{V_b} + K_{iv}X_v + K_{pv}V_b^* \end{cases} \tag{4}$$

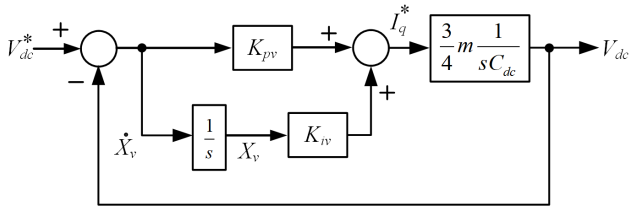

FIGURE 6. Block diagram of voltage loop control.

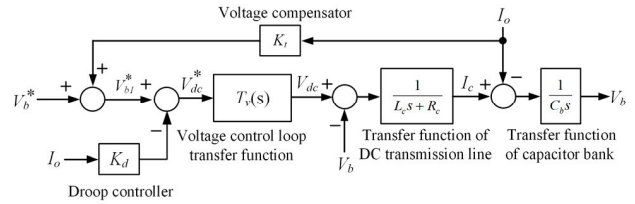

FIGURE 7. Block diagram of droop control and voltage compensation under voltage mode.

3) DROOP CONTROL AND VOLTAGE COMPENSATOR

Figure 7 depicts the block diagram of droop control and voltage compensation under voltage mode, in which the individual droop gain K_d of the droop controller is set equal to the global droop gain K_t [4]. This is because the power system investigated in this study is a single-generator/single-bus DC distribution MEA EPS. Under minimum transmission loss condition, the optimal gains K_t can be designed by using (12) and (13).

$$\begin{cases} \text{if } \dfrac{1}{3} \le r \le 1 \\ \quad R_L \dfrac{1-r}{1+r} < K_t \le \dfrac{R_L}{2}\left(\sqrt{1+\dfrac{1}{r}} - 1\right) \end{cases} \tag{12}$$

$$\begin{cases} \text{if } r > 1 \\ \quad 0 < K_t \le \dfrac{R_L}{2}\left(\sqrt{1+\dfrac{1}{r}} - 1\right) \end{cases} \tag{13}$$

where r is the ratio between the power of the CPL (P_{CPL}) and the resistive load (P_{R_L}).

For this study, $\zeta_i = 0.8$, $\zeta_v = 0.8$, $f_{ni} = 2000$ Hz, and $f_{nv} = 200$ Hz are selected to design the PI parameters of the current and voltage loops, and $P_{CPL} = 8$ kW and $P_{R_L} = 7$ kW are used to calculate the K_d and K_t gain for the droop control and voltage compensation, respectively. The resulting controller parameters of MEA EPS designed using the conventional design method are shown in Table 2.

B. ATS DESIGN METHOD

The methodology for designing the MEA EPS controller parameters using the ATS design method is described in this section. The ATS algorithm is selected for the optimal design because it can ensure convergence and escape the local solution [19], [22]. The ATS algorithm will search the controller

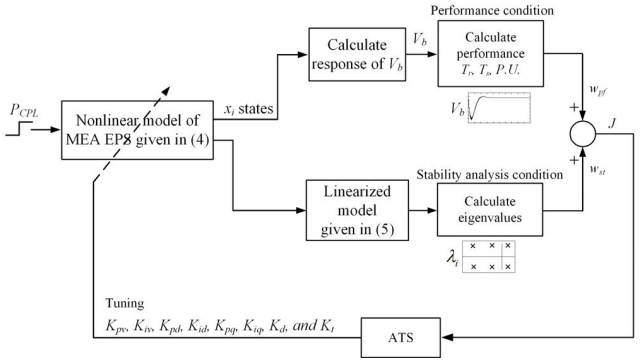

FIGURE 8. Process diagram for the optimal MEA EPS controller parameter design using the ATS design method.

parameters (K_{pd}, K_{id}, K_{pq}, K_{iq}, K_{pv}, K_{iv}, K_d, and K_t) until the optimal solution is obtained, resulting in the optimal output performance. A block diagram representing the process of optimal MEA EPS controller design by the ATS algorithm is shown in Fig. 8. To investigate system stability during the searching process, the eigenvalue theorem based on small-signal stability analysis is used as the penalty condition. The four steps of the design process are described in the remainder of this section.

Step 1: The operating range of MEA EPS is determined by defining the value of P_{CPL}. There are three conditions for setting P_{CPL}:

Condition 1: Changing P_{CPL} from 8 kW to 10 kW;
Condition 2: Changing P_{CPL} from 10 kW to 12 kW;
Condition 3: Changing P_{CPL} from 12 kW to 14 kW.

For the criteria of selecting these conditions, the minimum value of P_{CPL} must be more than one-third of P_{R_L} (7 kW/3 = 2.33 kW) [4] to achieve the minimum power loss. The maximum value of P_{CPL} must be less than 22 kW, which is the unstable margin of the considered system [16]. The sampling power for setting the conditions can be determined arbitrarily.

Step 2: The stability margin is assessed for all conditions in *Step 1*. The Jacobian matrix $\mathbf{A(x_0,u_0)}$ of the LTI dynamic model is expressed by substituting the system parameters given in Section I and the vector controller parameters from the ATS searching process into (5). The cost value for the penalty condition or stability analysis condition (w_{st}) is determined by (14). According to (14), if the system is unstable $Re\{\lambda\} \ge 0$, w_{st} is set to 10000 to eliminate these parameters to make the system unstable. However, if the system is stable, w_{st} is set to 0.

$$\begin{aligned} &if Re\{\lambda\} \ge 0 \\ &\quad w_{st} = 10000 \\ &\quad else \\ &\quad w_{st} = 0 \\ &\quad end \end{aligned} \tag{14}$$

Step 3: The V_b responses for all conditions in *Step 1* are calculated using the nonlinear model, which is expressed in (4). As in *Step* 2, the system parameters from Section I and the controller parameters randomly searched from the ATS are substituted into (4). The resulting V_b response is used to compute the cost value of the performance condition (w_{pf}) expressed by (15).

$$w_{pf} = \alpha\left(\frac{T_{r,ATS}}{T_{r,CON}}\right) + \beta\left(\frac{T_{s,ATS}}{T_{s,CON}}\right) + \gamma\left(\frac{P.U._{.ATS}}{P.U._{.CON}}\right) \tag{15}$$

where $T_{r,CON}$, $T_{s,CON}$, and $P.U._{.CON}$ are the rise time, setting time, and percent undershoot of V_b response when the system is controlled using the vector controller parameters designed by the conventional design method. $T_{r,ATS}$, $T_{s,ATS}$, and $P.U._{.ATS}$ are from the controller designed by the proposed ATS design method. The priority coefficients of T_r, T_s, and $P.U.$ are α, β, and γ, respectively, which are set to 0.33, 0.33, and 0.34, respectively. The sum of these coefficients must always be equal to 1.

Step 4: The stability analysis results and V_b response performances are assessed on the basis of cost value J calculated by (16). The ATS algorithm iteratively tunes the controller parameters K_{pd}, K_{id}, K_{pq}, K_{iq}, K_{pv}, K_{iv}, K_d, and K_t until J is minimized, indicating that the optimal V_b response performance is obtained with stable operation. The ATS parameters, i.e., initial number neighbor, number neighbor, radius, decreasing factor, and round, are set to 20, 40, 0.3, 1.4, and 50, respectively. The setting values of these parameters can be derived from a trial-and-error test under the condition of minimization of J. As for the defining boundary, the setting procedure is based on the conventional design: the upper and lower limits are, respectively, set to be 1.8 and 0.2 times the value of the controller parameters designed by the conventional design method. The resulting upper and lower limits of K_{pd}, K_{id}, K_{pq}, K_{iq}, K_{pv}, K_{iv}, K_d, and K_t are set to [−3.5810, −0.3979], [−3126.6906, −28140.2161], [−3.5810, −0.3979], [−3126.6906, −28140.2161], [0.7149, 6.4340], [561.4708, 5053.2375], [0.012, 0.108], and [0.012, 0.108], respectively.

$$J = \sum_{i=1}^{n} w_{pf,i} + w_{st,i} \tag{16}$$

where n is the number of operating conditions. It is set to 3 on the basis of Step 1.

The resulting controller parameters with their cost values represented by J and the convergence of J value are given in Table 2 and Fig. 9, respectively. Unlike the conventional design method, the ATS design method can provide the optimal DC bus voltage response (V_b). Figure 10 presents the theoretical stability analysis results when the ATS algorithm is used for the searching process. This figure shows that all solutions from the ATS algorithm can be confirmed for stable operation during the searching process. To verify

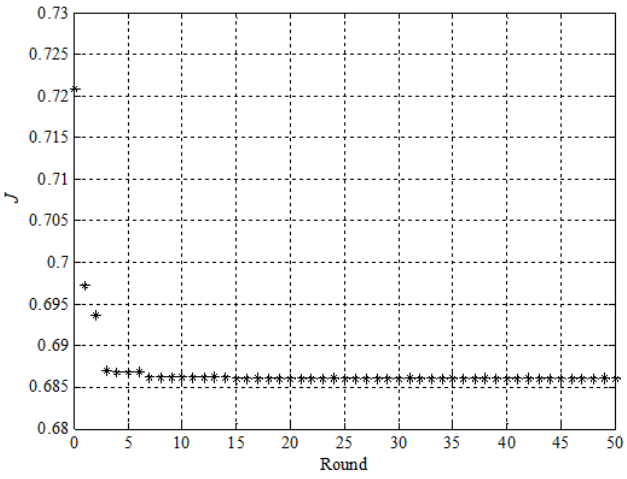

FIGURE 9. Convergence of J value from ATS design method.

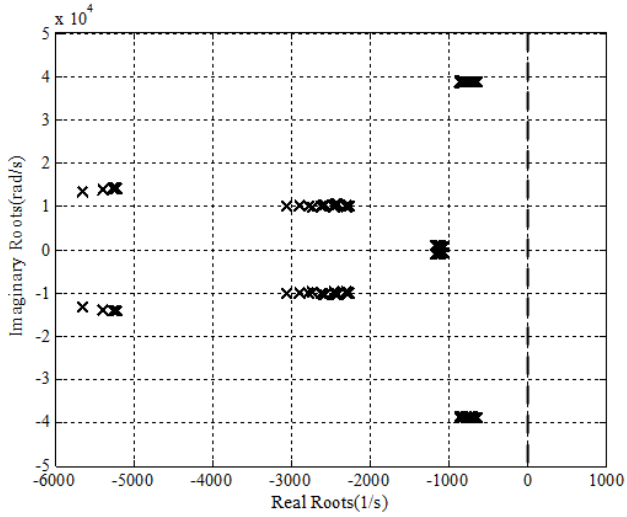

FIGURE 10. Dominant eigenvalue plot for the MEA EPS with the controllers designed using the ATS algorithm.

the proposed optimal design method, simulations using the MATLAB topology model and HIL technique are presented in Section V.

V. VERIFICATION BY MATLAB AND HIL SIMULATIONS

The proposed ATS design method can provide the optimal DC bus voltage response under stable operation conditions. In this section, the effectiveness of the controller designed using the ATS design method is validated through intensive time-domain simulations using MATLAB and HIL. For the HIL setup, Fig. 11 shows the connection between TMDSDOCK28335 board and the SimPowerSystem®in MATLAB. The MEA EPS controllers designed using the conventional and the ATS design methods are digitally embedded in a TMDSDOCK28335 board, and the remaining elements, depicted in Fig. 1, are contained in MATLAB. The V_b

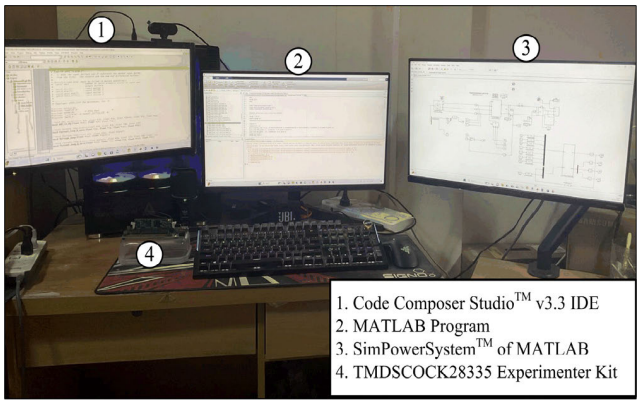

FIGURE 11. Connection between TMDSDOCK28335 board and the SimPowerSystem® in MATLAB.

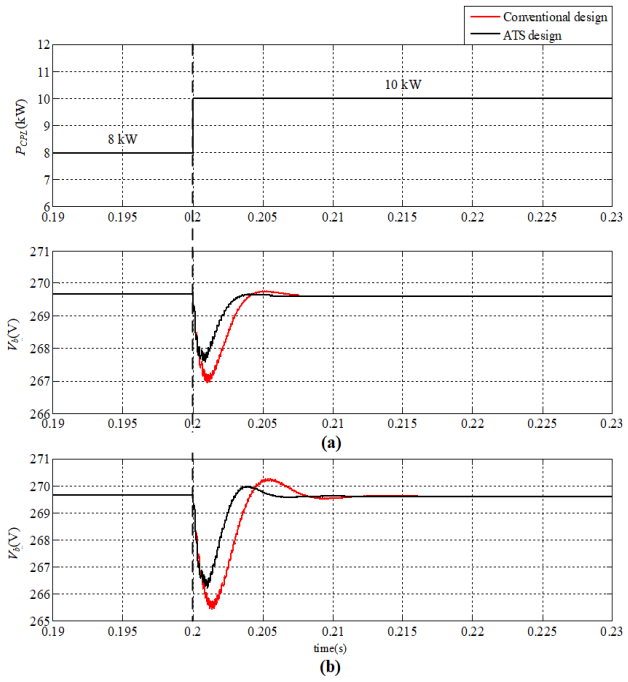

FIGURE 12. The resulting V_b waveforms under the condition of P_{CPL} changing from 8 to 10 kW. (a) MATLAB simulation results. (b) HIL simulation results.

waveforms corresponding to the conditions of changing P_{CPL} from 8 kW to 10 kW, from 10 kW to 12 kW, and from 12 kW to 14 kW are shown in Figs. 12, 13, and 14, respectively. Focusing on the transient responses, MATLAB and HIL simulations confirmed that the output performance of MEA EPS controllers designed by the proposed ATS design method is superior to that of MEA EPS controllers designed by the conventional design method in terms of rise time, setting time, and percent undershoot.

Overall, good agreement is observed among the theoretical results, MATLAB simulation results, and HIL simulation results under all three P_{CPL} variation conditions. Using the MEA EPS control system designed by the proposed ATS design method, the system operates stably and produces the optimal V_b response.

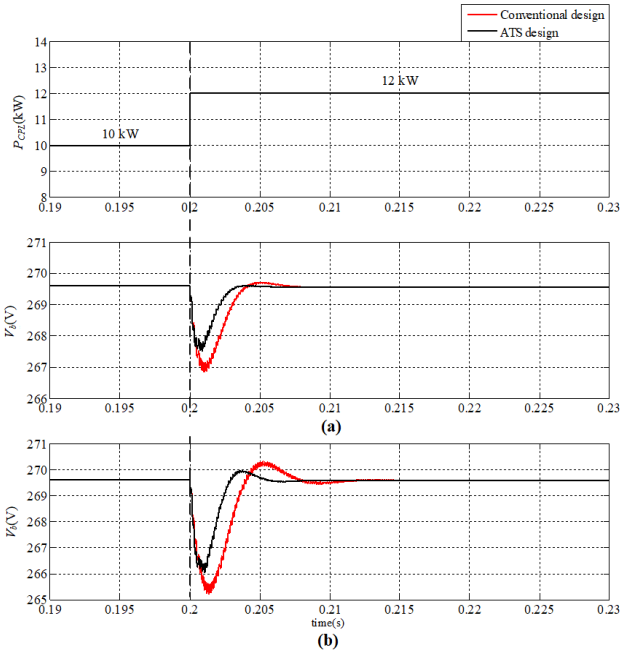

FIGURE 13. The resulting V_b waveforms under the condition of P_{CPL} changing from 10 to 12 kW. (a) MATLAB simulation results. (b) HIL simulation results.

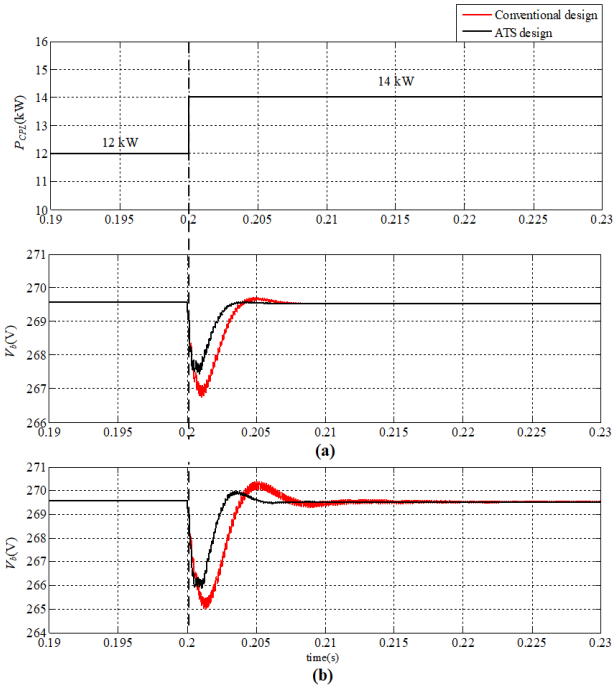

FIGURE 14. The resulting V_b waveforms under the condition of P_{CPL} changing from 12 to 14 kW. (a) MATLAB simulation results. (b) HIL simulation results.

VI. CONCLUSION

In this study, the ATS algorithm is applied to design controllers for the DC EPS of MEA. A modeling technique based on DQ transformation is applied to establish the state-variables-averaging model. The resulting nonlinear model can rapidly and accurately simulate the dynamic response to

evaluate DC bus voltage waveform (V_b) performance. For stability analysis during the design process, all eigenvalues are iteratively computed via the LTI dynamic model using a stability analysis technique based on the eigenvalue theorem. The results explicitly demonstrate that the MEA EPS under study maintains a stable state when the load conditions vary. The V_b response performance of the EPS is better with the controllers designed by the ATS design method than with the controllers designed using the conventional design method. These conclusions are validated by good agreement among the results of theoretical analysis, MATLAB simulations, and HIL simulations. Although the proposed algorithm can perform better than the conventional approach, it requires extra time for the search process. Furthermore, the proposed design method can aid in the controller design of other power systems such as bidirectional AC–DC inverters in electric vehicles and bidirectional voltage source converters in DC microgrid systems. In addition, instead of the proposed ATS algorithm, other AI algorithms, such as artificial bee colony, ant colony optimization, and flower pollination algorithms, can be used to design controllers by following the methodology used in this study. However, a drawback of the proposed technique is that if MEA EPS parameters or their operating points are varied, the controller parameters obtained from the ATS algorithm must be designed again following the process diagram shown in Fig. 8.

APPENDIX

The details of $\delta\mathbf{x}$, $\delta\mathbf{u}$, $\delta\mathbf{y}$, A, B, C, and D are can be expressed as follow:

$$\delta\mathbf{x} = \begin{bmatrix}\delta I_d & \delta I_q & \delta V_{dc} & \delta I_c & \delta V_b & \delta X_v & \delta X_{id} & \delta X_{iq}\end{bmatrix}^T$$
$$\delta\mathbf{u} = \begin{bmatrix}\delta I_d^* & \delta V_b^* & \delta P_{CPL}\end{bmatrix}^T$$
$$\delta\mathbf{y} = \begin{bmatrix}\delta V_{dc} & \delta I_c & \delta V_b\end{bmatrix}^T$$

$$a(2,5) = -\frac{K_{pv}K_{pq}(KK_t - K_d)}{L_q R_L} + \frac{K_{pv}K_{pq}P_{CPL}(K_t - K_d)}{L_q V_{b,0}^2}$$

$$a(3,1) = \frac{3}{2C_{dc}} \cdot \frac{1}{V_{dc,0}} \left(-2K_{pd}I_{d,0} + K_{id}X_{id,0} + K_{pd}I_d^*\right)$$

$$a(3,2) = \frac{3}{2C_{dc}} \cdot \frac{1}{V_{dc,0}} \left(-2K_{pq}I_{q,0} + \omega_e\phi_m - K_{pv}K_{pq}V_{dc,0} + K_{pv}K_{pq}V_b^* + \frac{K_{pv}K_{pq}(K_t - K_d)V_{b,0}}{R_L} + \frac{K_{pv}K_{pq}(K_t - K_d)P_{CPL}}{V_{b,0}} + K_{iq}X_{iq,0}\right)$$

$$a(3,3) = \frac{3}{2C_{dc}} \cdot \frac{1}{V_{dc,0}^2} \left(-K_{pd}I_{d,0}^2 + K_{id}I_{d,0}X_{id,0} + K_{pd}I_{d,0}I_d^* - K_{pq}I_{q,0}^2 + \frac{K_{pv}K_{pq}(K_t - K_d)I_{q,0}V_{b,0}}{R_L} + \frac{K_{pv}K_{pq}(K_t - K_d)P_{CPL}I_{q,0}}{V_{b,0}} + \omega_e\phi_m I_{q,0} + K_{iv}K_{pq}I_{q,0}X_{v,0} + K_{iq}I_{q,0}X_{iq,0} + K_{pv}K_{pq}I_{q,0}V_b^*\right)$$

$$a(3,5) = \frac{3K_{pv}K_{pq}(K_t - K_d)I_{q,0}}{2C_{dc}V_{dc,0}R_L} - \frac{3K_{pv}K_{pq}(K_t - K_d)P_{CPL}I_{q,0}}{2C_{dc}V_{dc,0}V_{b,0}^2}$$

$$a(8,5) = \frac{K_{pv}(K_t - K_d)}{R_L} - \frac{K_{pv}(K_t - K_d)P_{CPL}}{V_{b,0}^2}$$

$$\mathbf{B}(\mathbf{x_o}, \mathbf{u_o}) = \begin{bmatrix} -\frac{K_{pd}}{L_d} & 0 & 0 \\ 0 & -\frac{K_{pv}K_{pq}}{L_q} & -\frac{K_{pv}K_{pq}(K_t-K_d)}{L_q V_{b,0}} \\ \frac{3K_{pd}I_{d,0}}{2C_{dc}V_{dc,0}} & \frac{3K_{pv}K_{pq}I_{q,0}}{2C_{dc}V_{dc,0}} & \frac{3K_{pv}K_{pq}I_{q,0}(K_t-K_d)}{2C_{dc}V_{dc,0}V_{b,0}} \\ 0 & 0 & 0 \\ 0 & 0 & -\frac{1}{C_b V_{b,0}} \\ 0 & 1 & \frac{K_t-K_d}{V_{b,0}} \\ 1 & 0 & 0 \\ 0 & K_{pv} & \frac{K_{pv}(K_t-K_d)}{V_{b,0}} \end{bmatrix}_{8\times 3}$$

$$\mathbf{C}(\mathbf{x_0}, \mathbf{u_0}) = \begin{bmatrix} 0&0&0&0&0&0&0&0 \\ 0&0&0&0&0&0&0&0 \\ 0&0&1&0&0&0&0&0 \\ 0&0&0&1&0&0&0&0 \\ 0&0&0&0&1&0&0&0 \end{bmatrix}_{3\times 8}$$

$$\mathbf{A}(\mathbf{x_o}, \mathbf{u_o}) = \begin{bmatrix} \frac{K_{pd}-R_s}{L_d} & 0 & 0 & 0 & 0 & 0 & -\frac{K_{id}}{L_d} & 0 \\ 0 & \frac{K_{pq}-R_s}{L_q} & \frac{K_{pv}K_{pq}}{L_q} & 0 & a(2,5) & -\frac{K_{iv}K_{pq}}{L_q} & 0 & -\frac{K_{iq}}{L_q} \\ a(3,1) & a(3,2) & a(3,3) & -\frac{1}{C_{dc}} & a(3,5) & \frac{3K_{iv}K_{pq}I_{q,0}}{2C_{dc}V_{dc,0}} & \frac{3K_{id}I_{d,0}}{2C_{dc}V_{dc,0}} & \frac{3K_{iq}I_{q,0}}{2C_{dc}V_{dc,0}} \\ 0 & 0 & \frac{1}{L_c} & -\frac{R_c}{L_c} & -\frac{1}{L_c} & 0 & 0 & 0 \\ 0 & 0 & 0 & \frac{1}{C_b} & -\frac{1}{R_L C_b} + \frac{P_{CPL}}{C_b V_{dc,0}^2} & 0 & 0 & 0 \\ 0 & 0 & -1 & 0 & \frac{K_t-K_d}{R_L} - \frac{(K_t-K_d)P_{CPL}}{V_{b,0}^2} & 0 & 0 & 0 \\ -1 & 0 & 0 & 0 & 0 & 0 & 0 & 0 \\ 0 & -1 & -K_{pv} & 0 & a(8,5) & K_{iv} & 0 & 0 \end{bmatrix}_{8\times 8}$$

$$\mathbf{D}(\mathbf{x_0}, \mathbf{u_0}) = \begin{bmatrix} 0 & 0 & 0 \\ 0 & 0 & 0 \\ 0 & 0 & 0 \end{bmatrix}_{3\times 3}$$

REFERENCES

[1] K-N. Areerak, T. Wu, S. V. Bozhko, G. M. Asher, and D. W. P. Thomas, "Aircraft power system stability study including effect of voltage control and actuators dynamic," *IEEE Trans. Aerosp. Electron. Syst.*, vol. 47, no. 4, pp. 2574–2589, Oct. 2011.
[2] K. Areerak, S. V. Bozhko, G. M. Asher, L. De Lillo, and D. W. P. Thomas, "Stability study for a hybrid AC-DC more-electric aircraft power system," *IEEE Trans. Aerosp. Electron. Syst.*, vol. 48, no. 1, pp. 329–347, Jan. 2012.
[3] P. Wheeler and S. Bozhko, "The more electric aircraft: Technology and challenges," *IEEE Electrific. Mag.*, vol. 2, no. 4, pp. 6–12, Dec. 2014.
[4] F. Gao, S. Bozhko, G. Asher, P. Wheeler, and C. Patel, "An improved voltage compensation approach in a droop-controlled DC power system for the more electric aircraft," *IEEE Trans. Power Electron.*, vol. 31, no. 10, pp. 7369–7383, Oct. 2016.
[5] A. Barzkar and M. Ghassemi, "Electric power systems in more and all electric aircraft: A review," *IEEE Access*, vol. 8, pp. 169314–169332, 2020.
[6] A. Suyapan, K. Areerak, S. Bozhko, S. S. Yeoh, and K. Areerak, "Adaptive stabilization of a permanent magnet synchronous generator-based DC electrical power system in more electric aircraft," *IEEE Trans. Transport. Electrific.*, vol. 7, no. 4, pp. 2965–2975, Dec. 2021.
[7] T. Narongrit, K.-N. Areerak, and K.-L. Areerak, "Design of an active power filter using adaptive Tabu search," in *Proc. 8th WSEAS Int. Conf. Artif. Intell.*, Feb. 2009, pp. 314–318.
[8] T. Narongrit, K.-N. Areerak, and K.-L. Areerak, "Design of an active power filter using genetic algorithm technique," in *Proc. 9th WSEAS Int. Conf. Artif. Intell.*, Jan. 2010, pp. 46–50.
[9] K. Rojanaworahiran and K. Chayakulkheeree, "Real and reactive powers decomposition optimal power flow using particle swarm optimization," in *Proc. Int. Conf. Power, Energy Innov. (ICPEI)*, Oct. 2019, pp. 78–81.
[10] J. Soares, T. Sousa, Z. A. Vale, H. Morais, and P. Faria, "Ant colony search algorithm for the optimal power flow problem," in *Proc. IEEE Power Energy Soc. Gen. Meeting*, Jul. 2011, pp. 1–8.
[11] L. Wang, X. Zhang, and X. Zhang, "Antenna array design by artificial bee colony algorithm with similarity induced search method," *IEEE Trans. Magn.*, vol. 55, no. 6, pp. 1–4, Jun. 2019.
[12] R. Phosung, K. Areerak, T. Sopapirm, and K. Areerak, "Design and optimization of instability mitigation for AC–DC feeder systems with constant power loads using artificial intelligence techniques," *IEEE Trans. Power Electron.*, vol. 37, no. 5, pp. 5385–5397, May 2022.
[13] A. Emadi, "Modeling of power electronic loads in AC distribution systems using the generalized state-space averaging method," *IEEE Trans. Ind. Electron.*, vol. 51, no. 5, pp. 992–1000, Oct. 2004.
[14] A. Emadi, "Modeling and analysis of multiconverter DC power electronic systems using the generalized state-space averaging method," *IEEE Trans. Ind. Electron.*, vol. 51, no. 3, pp. 661–668, Jun. 2004.
[15] J. Pakdeeto, K. Areerak, S. Bozhko, and K. Areerak, "Stabilization of DC MicroGrid systems using the loop-cancellation technique," *IEEE J. Emerg. Sel. Topics Power Electron.*, vol. 9, no. 3, pp. 2652–2663, Jun. 2021.
[16] R. Phosung, K. Areerak, and K. Areerak, "Modeling and stability assessment of permanent magnet machine-based DC electrical power system in more electric aircraft," *Elect. Eng.*, vol. 105, pp. 3175–3190, Jun. 2023.
[17] A. Uan-Zo-li, R. P. Burgos, F. Lacaux, F. Wang, and D. Boroyevich, "Assessment of multipulse converter average models for stability studies using a quasistationary small-signal technique," in *Proc. 4th Int. Power Elect. Motion Control Conf.*, Aug. 2004, pp. 1654–1658.
[18] K. Areerak, T. Sopapirm, S. Bozhko, C. I. Hill, A. Suyapan, and K. Areerak, "Adaptive stabilization of uncontrolled rectifier based AC–DC power systems feeding constant power loads," *IEEE Trans. Power Electron.*, vol. 33, no. 10, pp. 8927–8935, Oct. 2018.
[19] D. Puangdownreong, K.-N. Areerak, S. Sujitjorn, and T. Kulworawanichpong, "Convergence analysis of adaptive Tabu search," *Int. J. Sci. Asia*, vol. 30, no. 2, pp. 183–190, Jul. 2009.
[20] *Aircraft Electric Power Characteristic*, Standard MIL-STD-704F, 2004. [Online]. Available: http://www.dodssp.daps.mil/
[21] T. Sopapirm, K.-N. Areerak, K.-L. Areerak, and A. Srikaew, "The application of adaptive Tabu search algorithm and averaging model to the optimal controller design of buck converters," *Int. J. Elect. Comput. Eng.*, vol. 5, no. 12, pp. 1707–1713, Dec. 2011.
[22] J. Pakdeeto, R. Chanpittayagit, K. Areerak, and K. Areerak, "The optimal controller design of buck-boost converter by using adaptive Tabu search algorithm based on state-space averaging model," *J. Electr. Eng. Technol.*, vol. 12, no. 3, pp. 1146–1155, May 2017.

RATAPON PHOSUNG received the B.Eng. (Hons.) and M.Eng. degrees in electrical engineering from the Suranaree University of Technology (SUT), Nakhon Ratchasima, Thailand, in 2018 and 2021, respectively. He is currently pursuing the Ph.D. degree in electrical engineering. From 2021 to 2022, he was a Researcher with the Institute of Research and Development, SUT. His main research interests include system identifications, artificial intelligence applications, stability analysis of power systems with constant power loads, modeling and control of power electronic-based systems, and control theory.

KONGPAN AREERAK (Member, IEEE) received the B.Eng. and M.Eng. degrees in electrical engineering from the Suranaree University of Technology (SUT), Nakhon Ratchasima, Thailand, in 2000 and 2001, respectively, and the Ph.D. degree in electrical engineering from the University of Nottingham, Nottingham, U.K., in 2009. In 2002, he was a Lecturer with the Electrical and Electronic Department, Rangsit University, Thailand. Since 2003, he has been a Lecturer with the School of Electrical Engineering, SUT. He was an Associate Professor of electrical engineering, in 2015. His research interests include system identifications, artificial intelligence applications, stability analysis of power systems with constant power loads, modeling and control of power electronic based systems, and control theory.

KONGPOL AREERAK (Member, IEEE) received the B.Eng., M.Eng., and Ph.D. degrees in electrical engineering from the Suranaree University of Technology (SUT), Thailand, in 2000, 2003, and 2007, respectively. Since 2007, he has been a Lecturer and the Head of the Power Quality Research Unit (PQRU), School of Electrical Engineering, SUT. He was an Associate Professor of electrical engineering, in 2015. His research interests include active power filter, harmonic elimination, AI application, motor drive, and intelligence control systems.